Classical description of the Electron Capture to the Continuum cusp formation in ion-atom collisions

Clara Illescas, B. Pons† and A. Riera

Laboratorio de Física Atómica y Molecular en Plasmas de Fusión Nuclear, asociado al Laboratorio de Fusión por Confinamiento Magnético, Departamento de Química, C-IX, Universidad Autónoma de Madrid,

Canto Blanco, 28049 Madrid, Spain

(December 5, 2001)

Abstract

Classical calculations are used to describe the dynamics of the Electron Capture to the Continuum (ECC) cusp formation in $H^+ + He$ collisions. We illustrate the frontier character of the ECC electrons between capture and ionization, and confirm that it is temporary capture, through projectile focusing, that is responsible for the ECC cusp. Furthermore, the cusp is not a divergence smoothed by the experiment, and is slightly shifted from the impact velocity value because of the residual pull from the target after ionization. This shift is the larger the smaller the nuclear velocity.

PACS number: 34.70.+e

One of the most outstanding features of ion-atom ionization cross sections is the electron capture to the continuum (ECC) cusp [1], that appears in the spectra of the emitted electrons in the forward direction ($\theta \sim 0^o$) when the velocity of the electron matches that of the projectile. The first theoretical explanations of this effect were in terms of a continuation across the ionization limit between electron capture and ionization [2], while most quantitative treatments have been carried out in the frame of perturbation theory [3,4,5]. A different contribution to the understanding of the mechanism came from Classical Trajectory Monte Carlo (CTMC, [6,7]) calculations, which allow a detailed picture of the process. In particular, Reinhold and Olson [8] (see also [9]) showed that the ECC peak can be considered as a classical phenomenon, and illustrated the cusp formation at different (long) times after the ionization event. They further showed that, at these large distances, electron-projectile interactions play an essential role in the formation of the cusp, and target-electron interactions in its asymmetry. The peak has also been shown to appear at non-zero degree emission angles both theoretically and experimentally [10].

In the present work we present a detailed classical description of the ECC cusp formation at zero degrees in H^+ + He collisions for impact energies ranging from 20 to 400 keV. Our statistics employ an ensemble of 10^6 electrons and differ from previous descriptions in that we employ:

(i) an impact parameter CTMC approach [11], which is amenable to graphical descriptions, and has been shown to yield accurate cross sections and probabilities [12] as well as spatial and momentum densities [13],

(ii) an initial distribution with average energy $U = 0.904$ a.u., that consists of a superposition of ten microcanonical ensembles [14], which was constructed so as to least-square fit a single-zeta Hartree-Fock function with effective charge $Z_{eff} = 1.6875$ [15]. Both spatial and momentum initial distributions are thus properly represented [16]. Collisional results are obtained in the frame of the independent particle model (IPM, [17,12]).

We identified the ECC electrons to the ionizing particles ejected within a solid angle $\theta \leq 1.5^0$ about the projectile direction at an internuclear distance $R_{max} = 2.10^6$ a.u.. In the following, atomic units are used unless otherwise stated; primed quantities refer to the frame of reference of the projectile and unprimed quantities to that of target.

In Fig. 1 we illustrate, as in ref. [18], the time evolution of the position and momenta (in the target frame of reference) of the ECC electrons along a nuclear trajectory with impact velocity $v = 2$ a.u. and impact parameter $b = 0.2$ a.u.. The overall behaviour of the electrons is very similar to that obtained in [18] for $b = 1.5$ a.u.; in fact, we generally found that the ECC mechanism does not significantly depend on the impact parameter, even though the contribution of ECC to the total ionization probability rapidly decreases with b.

The first step of the mechanism, near $Z = vt = 0$ a.u., is a polarization of the electron cloud towards the projectile. In the target frame used in Fig. 1, the ECC electrons are then subjected to a strong focusing effect induced by the projectile [19], that bends their trajectories in the longitudinal direction (see results for $Z = 5$ and 500 a.u. in Fig. 1). Besides the narrowing of the tranverse ECC momentum densities $\rho(p_x)$ and $\rho(p_y)$, this effect gives rise to a cusped shape in the longitudinal distribution $\rho(p_z)$, as shown in Fig. 2a.

In those early stages of the process, an overwhelming number of ECC electrons can be said to be temporarily captured by the projectile in Rydberg states, since their energy with respect to the projectile E'_P is small, and negative (see Fig. 2b). In the frame of the projectile, these electrons follow outward trajectories, and become progressively ionized (see Figs. 2): this shows the appropiateness of the heuristic picture [2] of ECC as a result of a continuation of electron capture above the ionizing threshold. To further illustrate this point, we compare in Fig. 3 the spatial location of all the ECC electrons with that of a large number of captured and ionized (mainly non-ECC) electrons that lie within a slab of width $\Delta p_y = 0.02$ a.u. about the (x, z) collision plane. The boundary between capture and ionization is approximately determined by a circumference, which has been drawn in Fig. 3 to illustrate our explanation; the same holds for the corresponding drawing in momentum space, except that the radius of the circle expands with time in coordinate space and shrinks in the latter.

This threshold property of ECC electrons beteween electron capture and ionization is commonly invoked to explain the cusped shape of the differential cross section and related distributions. For this purpose, one takes into account [20] that the electron capture cross section $d\sigma/dE'_P$ tends, in the accumulation point $E'_P = 0$, to a finite limit, which we have explicitly checked to be so in our classical calculations. Then, one considers continuation across the ionization threshold in the $r' \to \infty$ limit, so that $E'_P = p'^2/2$. Furthermore, since $d\mathbf{p}' = p'^2 dp' d\hat{p}'$, one obtains:

$$\frac{d\sigma}{p'dp'} = p' \int \frac{d\sigma}{d\mathbf{p}'} d\hat{p}' \tag{1}$$

so that $d\sigma/d\mathbf{p}' = d\sigma/d\mathbf{p}$ has a p'^{-1} singularity in the limit $p' \to 0$ -i.e., a $|\mathbf{p} - \mathbf{v}|^{-1}$ singularity in the $\mathbf{p} \to \mathbf{v}$ limit.

We found that this explanation applies nicely to our classical findings, and the only modifications are that the quantities p'^2 and r'^{-1} that are both made to tend to zero in the argument are of similar infinitesimal orders (in atomic units), so that one must *simultaneously*, and not sequentially, consider both limits. Then, instead of a singularity there results a peak (Fig. 2). In this respect, we checked that a singularity is *not* approached in the limit where the selection angle θ is progressively diminished, and the number of test particles increased accordingly. On the other hand, increasing the selection angle beyond 2^0 results in a decrease of the peak as may be expected.

In order to better understand the overall mechanism, it is useful to take into account that the ECC density spreads in an (approximately) symmetric way about the internuclear axis (see Fig. 1), with a centroid at $r \approx c \cdot R \approx c \cdot vt$, with $0.5 < c < 1$, depending mainly upon the nuclear velocity. Electrons become ionized at the time t_{ion} when their energy with respect to the projectile becomes positive. For electrons lying close to the centroid, the condition for ionization is:

$$E'_P(t_{ion}) = 0 = \frac{p'^2(t_{ion})}{2} - \frac{1}{r'(t_{ion})} \approx \frac{p'^2(t_{ion})}{2} - \frac{1}{(1-c)vt_{ion}} \tag{2}$$

We then obtain, in the target frame, since $p_z \gg |p_x|, |p_y|$ and $p_z(t_{ion}) \approx v + p'_z(t_{ion}) \approx v - p'(t_{ion})$:

$$\frac{p_z(t_{ion})}{v} \approx 1 - \frac{2^{1/2}}{(1-c)^{1/2} v^{3/2} t_{ion}^{1/2}} \tag{3}$$

This yields a $(t_{ion}, p_z(t_{ion}))$ curve whose $t^{-1/2}$ shape agrees with that of our calculations, shown in Fig. 4.

Since it has been repeatedly stressed that the ECC is a two-centre effect [19], and to elucidate the role of the nuclear centers on the subsequent evolution of the ECC cloud, we first neglect the pull from the target after ionization. The projectile-electron system is then stationary so that E'_P is conserved:

$$E'_P(t > t_{ion}) = \frac{p'^2(t)}{2} - \frac{1}{r'(t)} = 0. \tag{4}$$

As an illustration, we have drawn in Fig. 2b the density $\rho(E'_P)$ that is obtained when the electron-target interaction is abruptly and artificially cancelled at about the time $t \approx t_{ion}$ when the electron becomes ionized. According to equation (3), as $t \to \infty$ we have $r' \to \infty$, which yields $p' \to 0$ and $p \to v$. This is visible in Fig. 2a, where the corresponding ECC momentum density $\rho(p_z)$ shows a peak exactly at $p_z = v$. This peak is the sharper the numerically closer to t_{ion} is the time employed to disconnect the electron-target interaction. Hence, after ionization one-center (projectile) effects alone would result in a peak at $\mathbf{p} = \mathbf{v}$.

We now consider the additional effect of the other center (target ion), and find that the previous reasoning without target applies, with two modifications: i) the cusp of $\rho(p_z)$ peaks at smaller values, and although its position increases with time, its asymptotic value is slightly, but appreciably, less than v (see Fig. 2a); and ii) a tail appears at lower momenta (see Fig. 2a). While the latter feature ii) is well-known to be due to the field of the receding target on the outgoing electrons [19], the former one i) is new, and also originates from the pull from the target ion. This pull results in an acceleration of the electron departing from the projectile frame – hence, in a corresponding deceleration in the target frame of reference. The inspection of individual ECC trajectories shows that E'_P increases accordingly, yielding in the asymptotic region an energy distribution $\rho(E'_P)$ that peaks at $\delta E > 0$ (see Fig. 2b):

$$E'_P(t > t_{ion}) = \frac{p'^2(t)}{2} - \frac{1}{r'(t)} \approx \delta E. \tag{5}$$

As $t \longrightarrow \infty$ we have $r' \longrightarrow \infty$, that yields $E'_P(\infty) \longrightarrow \sqrt{2\delta E}$ and an asymptotic momentum density $\rho(p_z)$ with centroid at:

$$\frac{p_z}{v} \approx 1 - \frac{\sqrt{2\delta E}}{v} < 1, \tag{6}$$

in accordance with our asymptotic distribution of Fig. 2a.

Since post collisional effects such as i) and ii) above, resulting from the pull from the target ion, are strongly velocity-dependent, we now briefly comment on the changes in the mechanism with the nuclear velocity v. Taking $v = 4$ a.u. as an example of higher impact energies, and the same nuclear trajectory with impact parameter $b = 0.2$ a.u., we find that ionization takes place at smaller internuclear distances. For instance, most of the ECC electrons ionize at $t_{ion} < 5$ a.u. rather than < 50 a.u. as for $v = 2$ a.u. (see Fig. 4). Furthermore they are emitted with an higher velocity ($p_z(t_{ion})/v \approx 0.8$) and rapidly leave the target zone. The target pull on the ionizing electrons is thus less effective than the corresponding one at $v = 2$ a.u., yielding a smaller final shift of the ECC peak with respect to $p = v$ (see Fig. 5). As may be expected, the opposite holds at lower v, and we checked this by performing calculations down to $v = 0.89$ a.u. (see Fig. 5).

To sum up, classical results, and especially those obtained from impact parameter CMTC calculations with an improved initial condition, allow to integrate the equations of motion backwards in time to follow the behaviour of electrons that give rise to the ECC cusp. We have thus been able to illustrate for the first time the much discussed frontier character of these electrons, between capture and ionization, and see that it is indeed temporary capture, through projectile focusing, that is responsible for the cusp. After the first stage of the mechanism, which is a capture of the electron by the projectile, the process is best understood in the reference frame of the projectile. In this frame, the electronic motion is perturbed by the field of the receding target ion; this pull gives rise first to ionization, and then impresses a small, but finite, velocity with respect to the projectile. Furthermore, we find that the cusp is a peak and not a divergence smoothed by convolution over a small angle of acceptance in the experiment, so that the peak does not increase when this angle is diminished. Finally, because of the post collisional effect on the ionized electron, the cusp is slightly shifted from the $p = v$ value, and this shift is the larger the smaller the nuclear velocity. Finally these findings are in agreement with state-of-the-art recent measurements: from the experimental side, the suppression of the spurious low energy electrons together with careful shielding from the Earth's magnetic field of the energy analyser and the interaction region in the specially designed set up to obtain ECC electrons [21] has now allowed very precise measurements to be carried out to low energies. Such measurements of electron emission at zero degree in $H^+ + He$ and $H^+ + H_2$ collisions recently confirmed the shift [21]; as a token of this agreement, some raw data for the experimental doubly differential cross section are included in Fig. 2a. A full comparison requires, of course, integration of our calculated probabilities over all impact parameters. This will be presented in a separate publication, reporting a combined theoretical-experimental study of the energy dependence of the ECC peak.

ACKNOWLEDGMENTS

We thank Prof. M. B. Shah for useful discussions and for providing us with the experimental data of Fig. 2 prior to publication. This work has been partially supported by DGICYT Project No. SFM2000-0025. C. I. would like to acknowledge the Ministerio de Educación y Cultura, Spain, for financial support.

REFERENCES

[1] Crooks G. B. and Rudd M. E., Phys. Rev. Lett. **25** 1599 (1970)

[2] Rudd M. E. and Macek J. H., Case Stud. At. Phys. **3** 47 (1972)

[3] Salin A., J. Phys. B **2** 631 (1969)

[4] Macek J, Phys. Rev. A **1** 235 (1970)

[5] Fiol J., Rodríguez V. D. and Barrachina R. O., J. Phys. B **34** 933 (2001)

[6] Abrines R. and Percival I. C., Proc. Phys. Soc. London **88** 861 (1966)

[7] Olson R. E. and Salop A., Phys. Rev. A **16** 531 (1977)

[8] Reinhold C. O. and Olson R. E., Phys. Rev. A **39** 3861 (1989)

[9] Schultz D. R. and Reinhold C. O., Phys. Rev. A bf 50 2390 (1994)

[10] Sarkadi L., Brinkmann U., Báder A., Hippler R., Tökési K. and Gulyás L., Phys. Rev. A **58** 296 (1998)

[11] Bransden B. H. and McDowell M. H. C., *Charge exchange and the theory of ion-atom collisions* (Oxford Science Publications, Oxford 1992)

[12] Illescas C. and Riera A., Phys. Rev. A **60** 4546 (1999)

[13] Illescas C. Pons B. ans Riera A., Phys. Rev. A **63** 062722 (2001)

[14] Hardie D. J. W. and Olson R. E., J. Phys. B **16** 1983 (1983)

[15] Clementi E. and Roetti C., At. Data Nucl. Data Tables **14**, 177 (1974)

[16] Reinhold C. O. and Falcón C. A., J. Phys. B **21** 1829 (1988)

[17] McGuire J. H. and Weaver L., Phys. Rev. A **16** 41 (1977)

[18] McGrath C., McSherry D. M., Shah M. B., O'Rourke S. F. C., Crothers D. S. F., Montgomery G., Gilbody H. B., Illescas C. and Riera A., J. Phys. B **33** 3693 (2000)

[19] Stolterfoht N., DuBois R. D. and Rivarola R. D., *Electron Emission in Heavy Ion-Atom Collisions*, subsection 5.3.1 (Springer Verlag, Berlin 1997) *and references therein*

[20] Fiol J., Courbin C., Rodríguez V. D. and Barrachina R. O., J. Phys. B **33** 5343 (2000)

[21] McGrath C., Shah M. B., McSherry D. M., O'Rourke S. F. C., Crothers D. S. F., Gilbody H. B., Illescas C. and Riera A., *Abstracts of contributed papers of XXII-ICPEAC*, edited by S. Datz *et al.*, Rinton Press (2001)

† *permanent address*: CELIA, UMR 5107 du CNRS, Université de Bordeaux-I, 351 Cours de la Libération, F-33405 Talence, France.

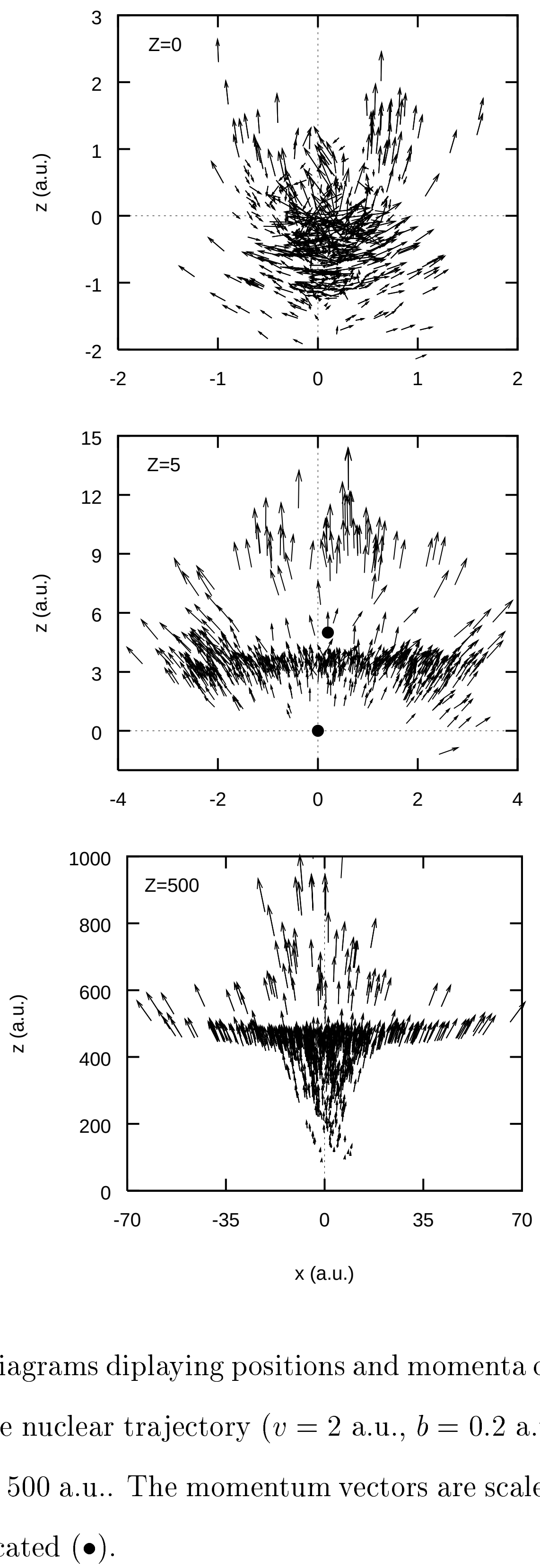

Figure 1: Arrow diagrams diplaying positions and momenta of the ECC electrons in $H^{+}+He$ collisions along the nuclear trajectory ($v = 2$ a.u., $b = 0.2$ a.u.), for internuclear coordinates $Z = vt = 0$, 5 and 500 a.u.. The momentum vectors are scaled for sake of clarity and nuclear positions are indicated ($\bullet$).

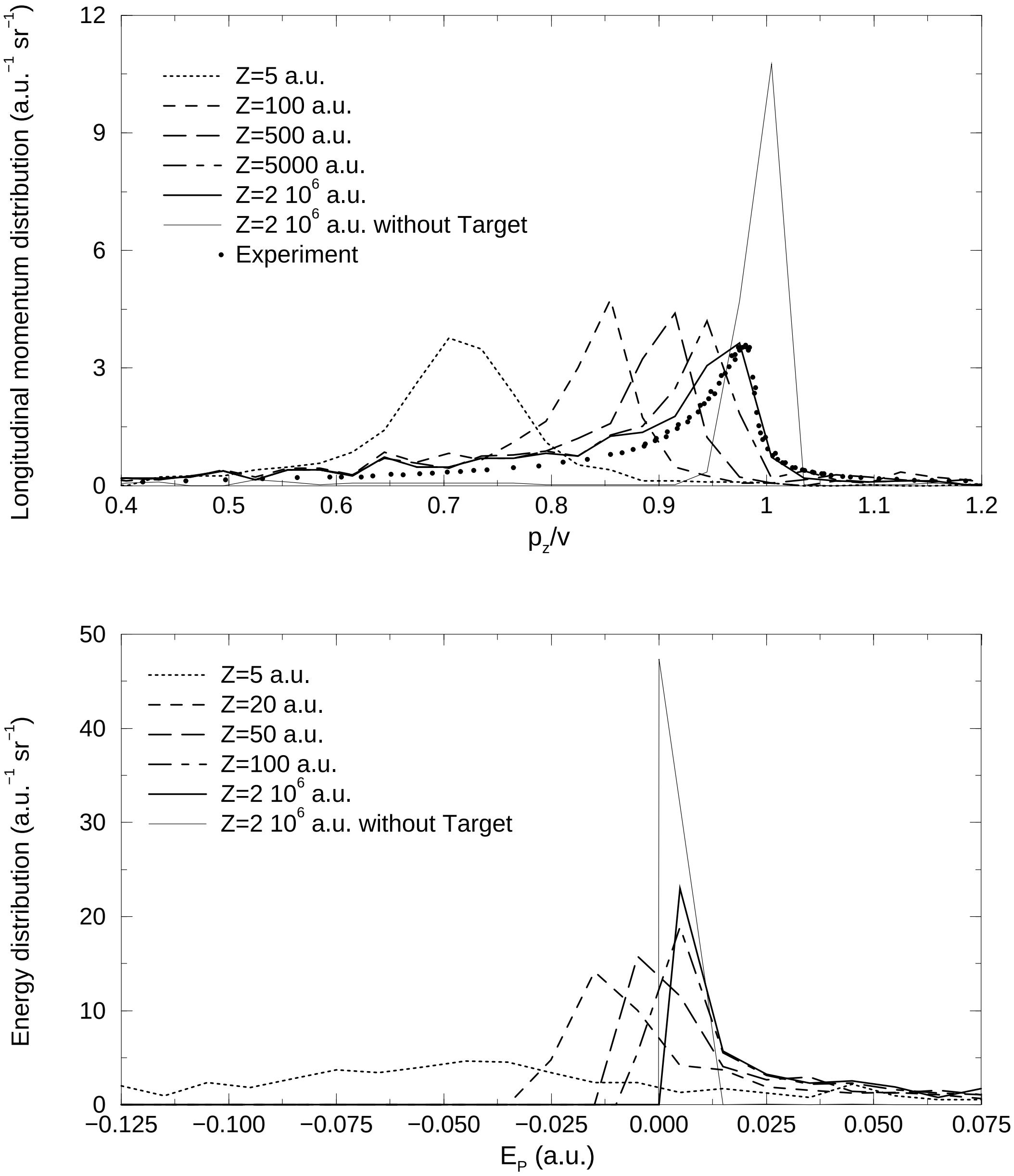

Figure 2: Time evolution of the longitudinal momentum (2a) and projectile energy (2b) distributions for the ECC electrons in $H^+ + He$ collisions along the nuclear trajectory ($v = 2$ a.u., $b = 0.2$ a.u.). (Arbitrarily normalized) experimental data [21] for the double differential cross section at zero degree emission are included in Fig. 2a.

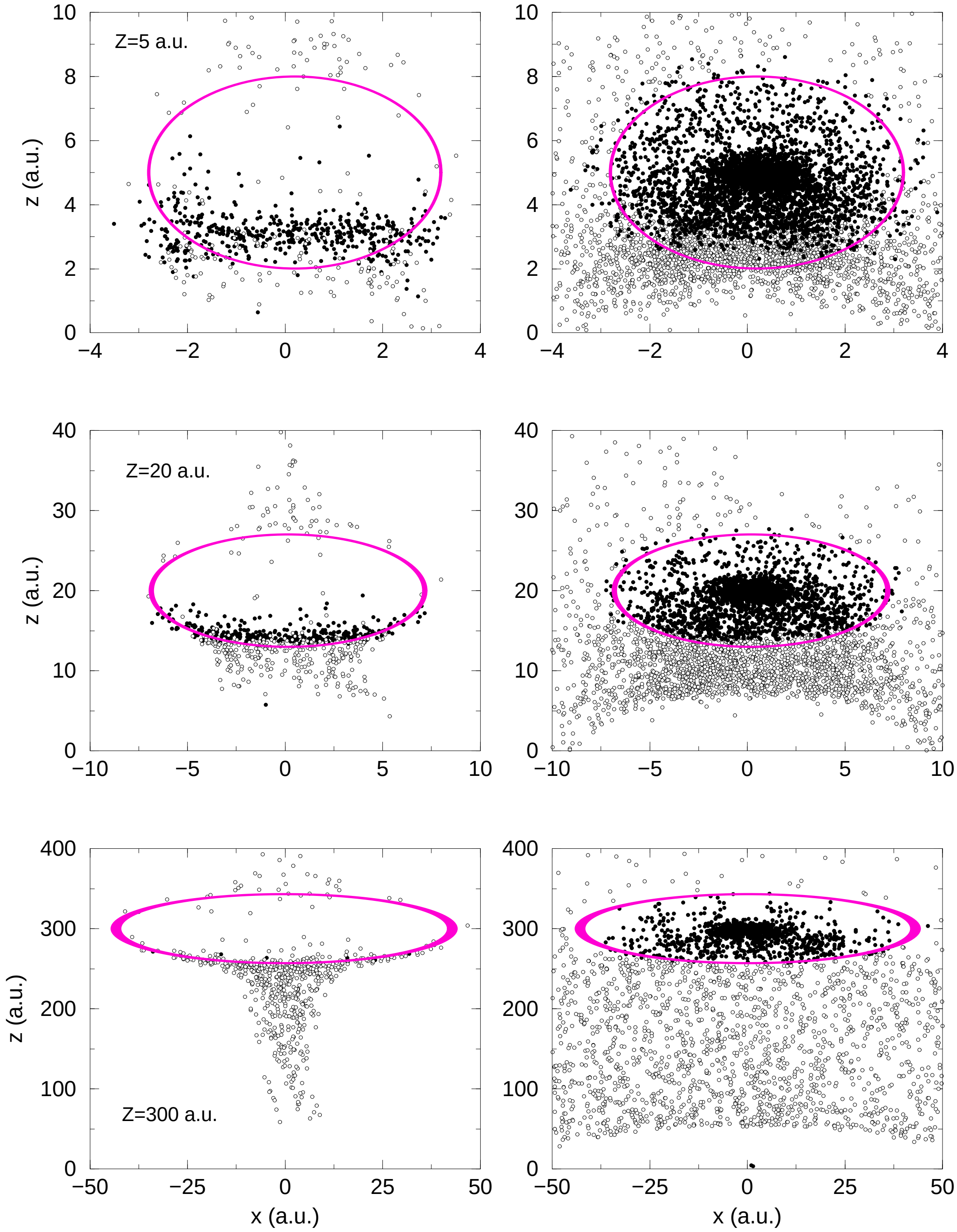

Figure 3: Time evolution of the positions of ECC electrons (left column) and of ionized (∘) and captured (•) electrons (right column). We have drawn approximatively the frontier between the ionizing and capture clouds in both columns to emphasize the threshold property of ECC electrons.

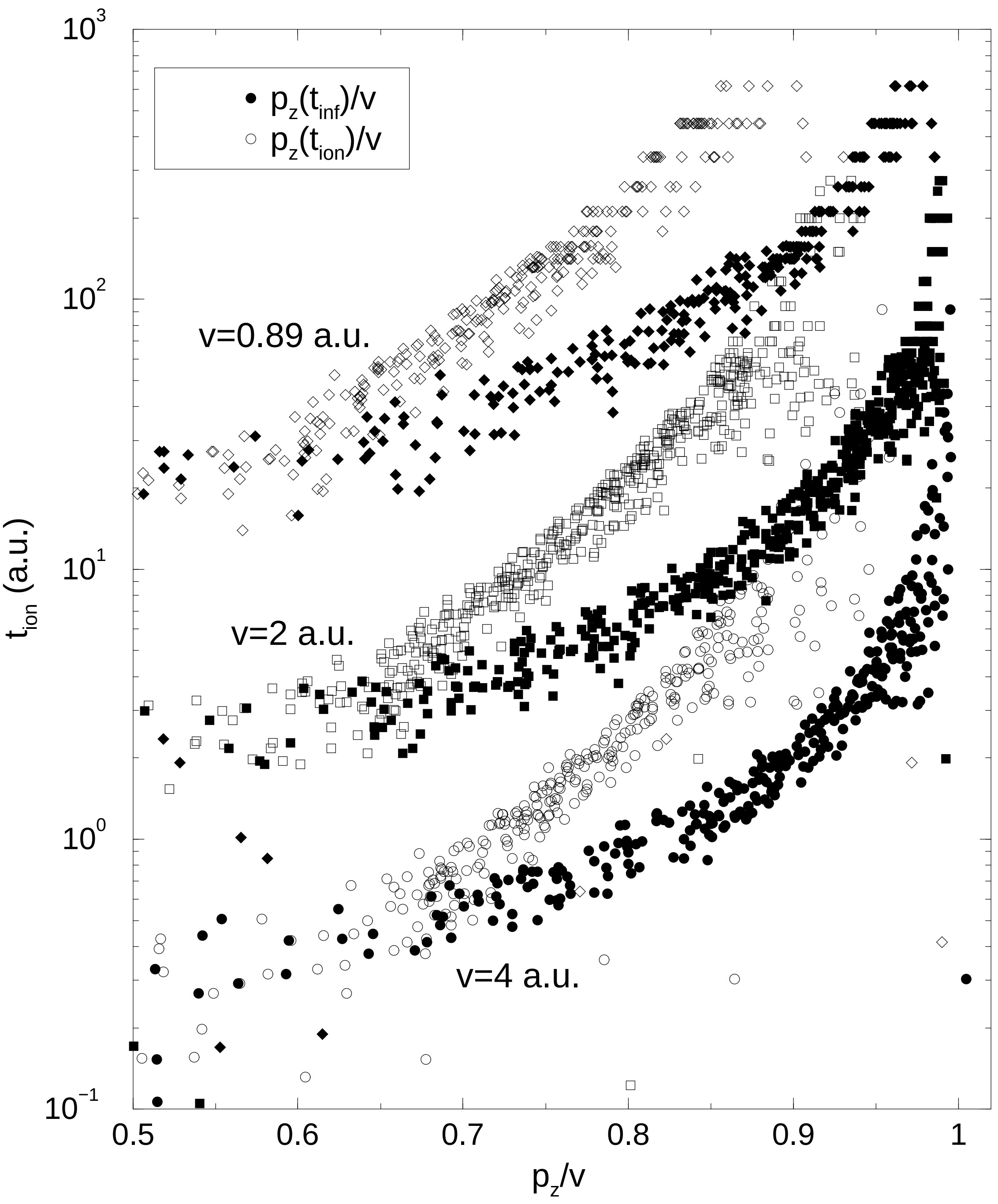

Figure 4: Scaled longitudinal momenta of ECC electrons at time of ionization $p_z(t_{ion})/v$ and at final time of integration $p_z(t_{inf})/v$ for different impact velocities and impact parameter $b = 0.2$ a.u..

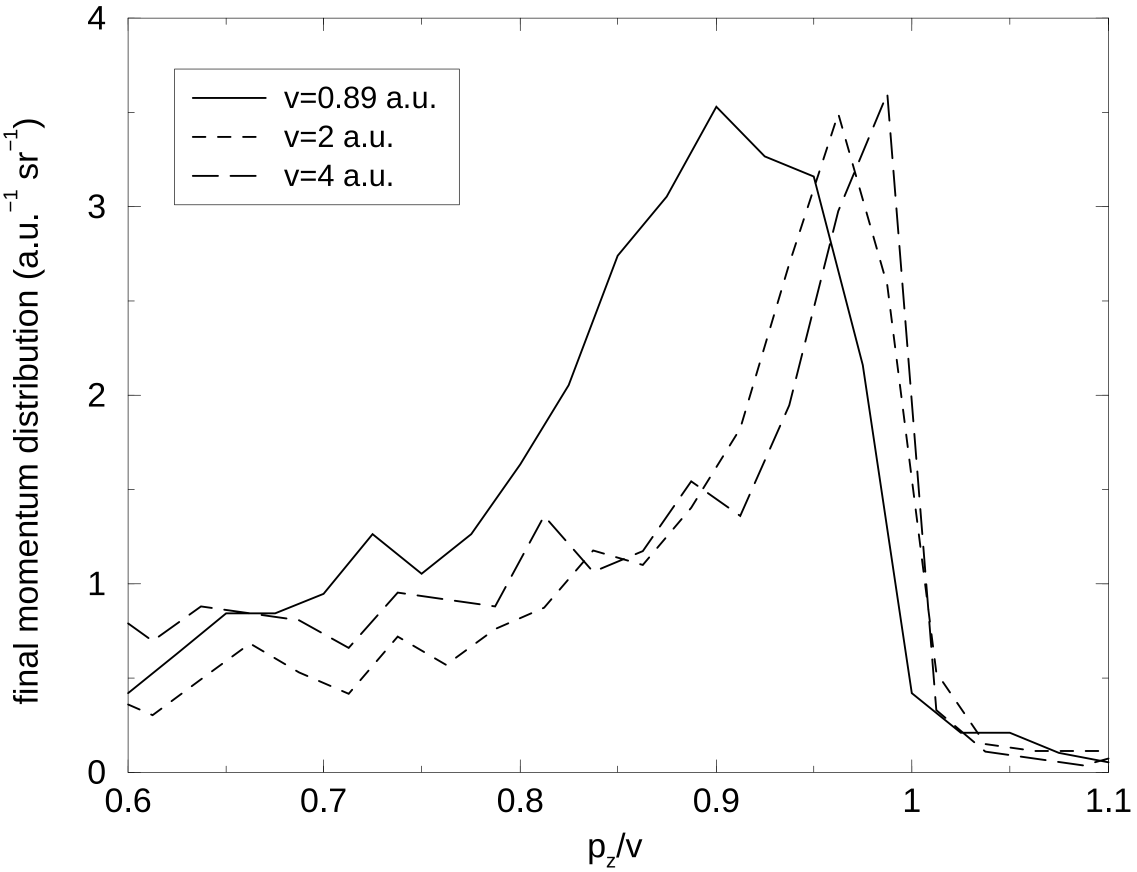

Figure 5: Asymptotic longitudinal momentum distributions for different impact energies $E = 20$, 100 and 400 keV and impact parameter $b = 0.2$ a.u.. The $E = 20$ and 400 keV distributions have been arbitrarily scaled with respect to the 100 keV one to make clearer the energy dependence of the ECC shift.